Terahertz waveguiding between parallel dielectric films

Yi Pan[1,2] and Steven R. Andrews[1*]

[1]Department of Physics, University of Bath, Claverton Down, Bath BA2 7AY, UK
[2]Currently with the School of Engineering and Computer Sciences, Durham University, South Rd, Durham DH1 3LE, UK
[*]s.r.andrews@bath.ac.uk

Abstract: We report a study of terahertz waveguiding between parallel dielectric films, a system that can be viewed as a planar analogue of hollow core fibres that exploit anti-resonant reflection optical waveguiding (ARROW). With the aid of time domain waveguide mode imaging, the frequency dependent transition from ARROW to total internal reflection guiding in the individual films as the film separation is reduced and the effect on the transmission of adding variably spaced cladding layers are clearly revealed. Good agreement for the transmission, dispersion and loss is obtained with simple analytical models for film separations greater than about five wavelengths suggesting that the same models could be usefully used to predict the behaviour in the case of the technologically more important cylindrical geometry.

OCIS codes: (230.7370) Waveguides; (130.2790) Guided waves; (300.6495) Spectroscopy, terahertz.

References and links

1. M. Tonouchi, "Cutting edge terahertz technology," Nat. Photon. **1**, 97-105 (2007).
2. X.-C. Zhang and J. Xu, *Introduction to THz Wave Photonics* (Springer, 2010).
3. S. R. Andrews, "Microstructured Terahertz Waveguides," J. Phys. D: Appl. Phys. **47**, 374004 (2014).
4. S. Atakaramians, S. Afshar V., T. M. Monro, and D. Abbott, "Terahertz dielectric waveguides," Adv. in Opt. and Photon. **5**, 169-215 (2013).
5. R. W. McGowan, G. Gallot and D. Grischkowsky, "Propagation of ultra-wide band, short pulses of THz radiation through sub-mm diameter circular waveguides," Opt. Lett. **24**, 1431-1433 (1999)
6. R. Mendis and D. Grischkowsky, "Undistorted guided-wave propagation of subpicosecond terahertz pulses," Opt. Lett., **26**, 846-848 (2001).
7. M. Wächter, M. Nagel and H. Kurz, "Metallic slit waveguide for dispersion-free low-loss terahertz signal transmission," Appl. Phys. Lett. **90**, 061111 (2007).
8. B. Bowden, J. A. Harrington and O. Mitrofanov, "Silver/polystyrene-coated hollow glass waveguides for the transmission of terahertz radiation," Opt. Lett. **32**, 2945-2947 (2007).
9. C.-H. Lai, Y.-C. Hsueh, H.-W. Chen, Y.-J. Huang, H.-C. Chang, and C.-K. Sun, "Low-index terahertz pipe waveguides," Opt. Lett. **34**, 3457-3459 (2009).
10. J.-Y. Lu, C.-P. Yu, H.-C. Chang, H.-W. Chen, Y.-T. Li, C.-L. Pan, and C.-K. Sun, "Terahertz air-core microstructure fiber," Appl. Phys. Lett. **92**, 064105 (2008).
11. J. Anthony, R. Leonhardt, S. G. Leon-Saval, and A. Argyros, "THz propagation in kagome hollow-core microstructured fibers," Opt. Express **19**, 18470-18478 (2011).
12. L. Vincetti, "Numerical analysis of plastic hollow core microstructured fiber for terahertz applications," Opt. Fiber Tech., **15**, 398 (2009).
13. N. M. Litchinister, A. K. Abeeluck, C. Headley, and B. J. Eggleton, "Antiresonant reflecting photonic crystal optical waveguides," Opt. Lett. **27**, 1592-1594 (2002).
14. S. Fevrier, B. Beaudou, and P. Viale, "Understanding origin of loss in large pitch hollow-core photonic crystal fibers and their design simplification," Opt. Express **18**, 5142-5150 (2010).
15. M. A. Duguay, Y. Kokubun, T. L. Koch, and L. Pfeiffer, "Antiresonant reflecting optical waveguides in SiO_2-Si multilayer structures," Appl. Phys. Lett. **49**, 13-15 (1986).
16. F. Yu, W. J. Wadsworth, and J. C. Knight, "Low loss silica hollow core fibers for 3-4 μm spectral region," Opt. Express **20**, 11153-11158 (2012).

17. B. Beaudou, F. Gerôme, Y. Y. Wang, M. Alharbi, T. D. Bradley, G. Humbert, J.-L. Auguste, J.-M. Blondy, and F. Benabid, "Millijoule laser pulse delivery for spark ignition through kagome hollow-core fiber," Opt. Lett. **37**, 1430-1432 (2012).
18. A. N. Kolyadin, A. F. Kosolapov, A. D. Pryamikov, A. S. Biriukov, V. G. Plotnichenko, and E. M. Dianov, "Light transmission in negative curvature hollow core fiber in extremely high material loss region," Opt. Express **21**, 9514-9519 (2013).
19. O. Mitrofanov, T. Tan, P. R. Mark, B. Bowden, and J. A. Harrington, "Waveguide mode imaging and dispersion analysis with terahertz near-field microscopy," Appl. Phys. Lett. **94**, 171104 (2009)
20. HiFi Industrial Films Ltd., Stevenage SG1 4SX, UK.
21. Y.-S. Jin, G.-J. Kim, and S.-G. Jeon, "Terahertz dielectric properties of polymers," J. Korean Phys. Soc., **49**, 513-517 (2006).
22. M. Misra, Y. Pan, C. R. Williams, S. A. Maier, and S. R. Andrews, "Characterization of a hollow core fibre-coupled near field terahertz probe," J. Appl. Phys. **113**, 193104 (2013).
23. M. Miyagi and S. Nishida, "A proposal of low-loss leaky waveguide for submillimeter waves transmission," IEEE Trans. MTT **28**, 398-401 (1980).
24. E. A. J. Marcatili and R. A. Schmeltzer, "Hollow metallic and dielectric Wwveguides for long distance optical transmission and lasers," Bell Syst. Tech. J. **43**, 1783-1809 (1964).
25. F. Gerôme, R. Jamier, J.-L. Auguste, G. Humbert, and J.-M. Blondy, "Simplified hollow-core photonic crystal fiber," Opt. Lett. **35**, 1157-1159 (2010).
26. F. Poletti, J. R. Hayes, and D. Richardson, "Optimising the performances of hollow antiresonant fibres," in OSA Technical Digest (CD), Optical Society of America, Washington (2011).
27. R. Mendis and D. Grischkowsky, "Plastic ribbon THz waveguides," J. Appl. Phys. **88**, 4449-4451 (2000)
28. M. Tacke and R. Ulrich, "Submillimeter wave-guiding on thin dielectric films," Opt. Commun. **8**, 234-238 (1973).

1. Introduction

Research involving the tetrahertz (THz) part of the electromagnetic spectrum, commonly taken to be that lying between 0.1 and 10 THz (3 mm to 30 μm), has seen rapid growth in recent years because of the importance of THz radiation as a low energy probe of the optical properties and dynamics of matter and because of emerging real world applications in areas as diverse as industrial quality control, biosensing and security screening [1,2]. Despite a vigorous growth in THz technology, many components and processes taken for granted at higher and lower frequencies are still in an early stage of development. One example of this is the use of waveguides to transport or spatially confine radiation [3,4]. There has been much recent interest in the use of hollow guiding structures because this allows some isolation from external perturbations and because if radiation is mostly confined to dry air in the core then the effects of material absorption and dispersion, which tend to be significant at THz frequencies, are reduced. Examples in which by far the greater fraction of radiation is guided in air include metallic tubes [5], parallel plates [6] and slot guides [7], dielectric coated metal tubes [8], thin wall polymer tubes [9] and micro-structured polymer fibres [10-12].

Hollow all-dielectric guides with core diameters larger than the wavelength do not generally support guiding by total internal reflection and, with the notable exception of fibres exploiting photonic bandgap cladding, there are no true guided modes. Propagation in thin-walled, hollow tubes and microstructured hollow core fibres (MOFs) in which the core is surrounded by one or more concentric rings of tubes within an outer jacket, instead takes place via grazing incidence reflection [13,14]. This mechanism only supports leaky modes which gradually lose energy to the surrounding cladding and radiation and is commonly referred to as anti-resonant reflecting optical waveguiding (ARROW). This description refers to the dramatic increase in loss at frequencies corresponding to Fabry-Perot transmission resonances in the cladding walls [15]. Although leaky and particularly susceptible to bending loss, hollow core ARROW guides are useful because they can have moderately low attenuation when the core diameter is large compared with the wavelength and the wall thickness is small. For example losses as low as a few dB/m over a 1 THz range near 1 THz have been reported in microstructured polymer tubes with cores 4 to 5 mm in diameter [4,10], which is comparable with that expected from a similar size parallel plate copper waveguide [4] and not much higher than that obtained for dielectric lined metal tubes (~ 1 dB/m for a 2

mm core [8]). An important characteristic of ARROW guides is that it is possible to engineer very low field overlap with the dielectric. In silica MOFs this allows the transport of high power radiation [16] and guiding at wavelengths where dielectric absorption is significant, such as in the mid infrared [17,18]. Analytical models to describe dispersion and attenuation in such guides are desirable for simplifying the solution of pulse propagation equations in nonlinear optics and as an alternative to computationally expensive finite element wave propagation solvers in the linear case so that it is useful to verify their practical limits of applicability experimentally. In cylindrical symmetry systems the core diameter and wall thickness cannot easily be varied independently to study details of the guidance experimentally because of limitations of the usual capillary and fibre drawing techniques. Here, we demonstrate that a planar terahertz analogue of such cylindrical symmetry guides based on parallel dielectric films can serve as an aid to understanding the breakdown of leaky mode guidance and the effect of air-spaced cladding layers because the structural parameters can be systematically varied and studied in detail using time domain waveguide mode imaging [19].

2. Parallel film waveguides

We used two identical, thin polyester (polyethylene terephthalate) films [20] of 13.5 cm length and 6 cm width, stretched tight over rigid plastic frames to make a parallel dielectric film waveguide. Similar films are readily available under the trade name of Mylar. In later studies two 6 mm thick, high density polyethylene (HDPE) sheets were used to add extra cladding to the basic waveguide to make a simplified planar analogue of cylindrical anti-resonant reflective fibre [13]. The refractive index and absorption coefficient of the polyester films were determined in transmission by means of standard time domain THz spectroscopy (TDTS) measurements on thick films and found to be 1.59±0.05 and 18±2 cm^{-1} near 1 THz and only weakly frequency dependent. The refractive index and absorption coefficients of nominally similar polyester at 1 THz are reported to be about 1.7 and 25 cm^{-1} respectively [21]. The measured refractive index and absorption coefficient of the HDPE were 1.53 and 2 cm^{-1} near 1 THz. Although the absorption coefficient of polyester is an order of magnitude higher than for HDPE or polytetrafluoroethylene (PTFE), the films are mechanically robust and uniform in thickness to within ±1 μm. The films were mounted on translation stages to achieve a variable separation. The geometry of the TDTS experiment is shown in Fig. 1.

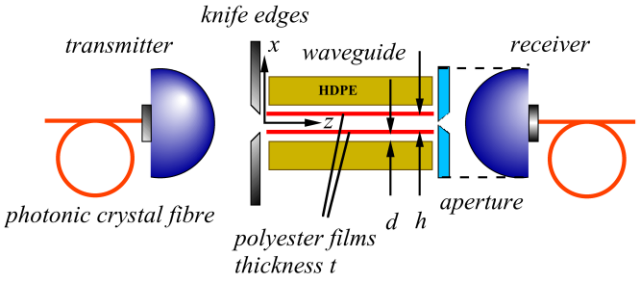

Fig. 1. The experimental TDTS geometry. The field incident on the waveguide, which is made from two parallel polyester films of thickness t and separation h, is polarized along x. In some experiments outer cladding layers of HDPE or a receiver aperture are added, as shown.

A 3 THz maximum usable bandwidth TEM_{00} beam with electric field along the x-axis and a diameter of 7 mm (FWHM) was launched along the z-axis from a 12 mm diameter aspheric silicon collimating lens attached to a hollow core fibre-coupled GaAs photoconductive transmitter so as to excite the fundamental TM_0 core mode of a 13.5 cm long waveguide. Although we only discuss this particular mode here, qualitatively similar behavior is also observed when exciting the TE_0 mode. Knife edges were used to define an input aperture similar in width to the film separation in order to minimize detection of unguided radiation. A fibre-coupled low temperature GaAs photoconductive receiver with a 10 μm long dipole

antenna was used for coherent detection. The fibre-coupled apparatus has been described previously [22]. In some experiments a piece of 0.5 mm thick copper clad circuit board pierced by a 200 μm diameter circular aperture was attached to the front of the receiver lens. The receiver assembly was mounted on motorized translation stages and could thus be used to perform spatially resolved coherent detection, typically in a plane less than 100 μm from the output end of each guide. The aperture had an effective low frequency cut-off near 0.2 THz.

Figure 2(a) shows transmitted time domain signals collected without an aperture and with the collection lens centered on the optical axis (i.e. at x=0) for different film thicknesses of 50 and 100 μm and the same separation of 2.0 mm. In both cases, it can be seen that the guided wave exhibits anomalous dispersion, where the higher frequency signal components travel faster than those at lower frequency, and the sub-ps input pulse broadens by several ps. The spectra of the time domain signals are shown in Fig. 2(b). For the waveguide constructed with 50 μm thick films, a transmission window is visible between approximately 0.7 THz and 2 THz. Core mode guidance appears to break down below 0.6 THz but there is evidence of a weak transmission window at lower frequency which is associated with guiding in the cladding films and discussed further in section 3. In the case of the 100 μm thick films, a loss band associated with resonant transmission through the films is obvious near 2.2 THz.

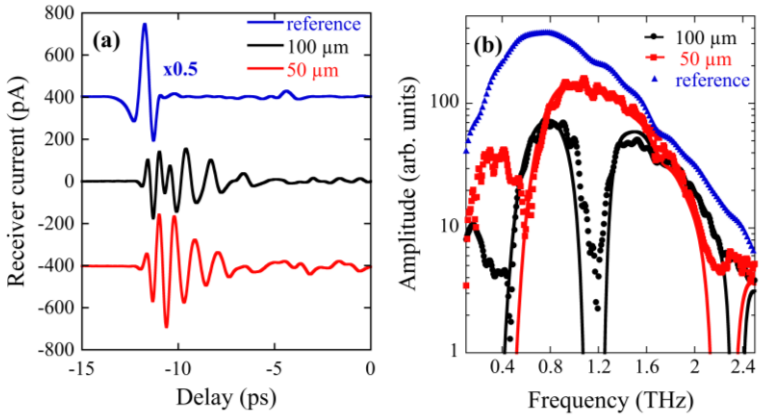

Fig. 2. (a) Time domain traces obtained after propagation between two parallel polyester films with the film thicknesses shown. The film separation is 2.0 mm and the length is 13.5 cm. The reference signal shows the signal obtained by removing the waveguide. (b) Amplitude spectra (symbols) of the traces in (a). The solid curves are calculated using Eq. (1) and the reference transmission spectrum.

For film thickness t and separation h the amplitude attenuation coefficient α_E for leaky TM_m modes can be calculated using a transverse transmission line model described by Miyagi and Nishida [23]. In the $\lambda/h<<1$ limit the result is

$$\alpha_E = \frac{1}{\nu^2}\left[\frac{(n^2-1)n^4 k_o u_\infty^3}{\nu^2 \sin^2(2\nu t/h) + 4u_\infty^2}\right]\left(1+\frac{k_o h t}{2nu_\infty}\alpha_d\right). \qquad (1)$$

In Eq. (1) n is the film refractive index, k_o is the free space wavevector, $\nu = k_o t\sqrt{(n^2-1)}$ is the normalized frequency and $u_\infty = (m+1)\pi/2$. The mode index m is equal to the number of peaks of electric field intensity in the interval $0 < x < h/2$. The term in square brackets in Eq. (1) describes transmission through the films, which behave like Fabry-Perot cavities, and the term in round brackets accounts for dielectric loss in a first order perturbation analysis where α_d is the dielectric power absorption coefficient and it is assumed that $\alpha_d/(nk_o) << 1$.

Equation (1) can be applied to thin walled tubes simply by substituting the diameter for h and the m^{th} root of $J_1(x)$ (except zero) for u_∞.

Very high loss from the core modes occurs at frequencies where the denominator of Eq. (1) is a minimum. The centre frequencies of these loss bands, f_p, are given by

$$f_p = \frac{pc}{2t\sqrt{n^2 - 1}} \tag{2}$$

where p=1,2,3… . The frequencies f_p also correspond to both resonant transmission through the films and the cut-offs of TM_p modes guided by total internal reflection in the films with p peaks in electric field intensity in the region $h/2 < x < h/2+t$. Below cut-off, these modes can satisfy the phase matching condition for coupling to core modes and are responsible for leakage of energy away from the core. Above cut-off, in thin films the fields extend large distances into the surrounding air so that they have the character of surface modes. For convenience, we shall use this description hereafter. The frequencies for minimum core leakage are found between the resonant loss frequencies, where the guiding is 'anti-resonant'. Ignoring dielectric loss, the minimum attenuation in these regions predicted by Eq. (1) scales as $(m+1)^3 \lambda^3 / h^4$ if $\nu >> u_\infty$. The transmission thus decreases dramatically with increasing λ/h and there is strong suppression of higher order modes, leading to single mode propagation for modest guide lengths. These effects can both be understood from the relationship between λ/h and the grazing angle of incidence, $\theta \approx \sin^{-1}(\lambda / 2h)$; small θ and therefore small λ/h and low mode order are essential for a large reflection coefficient.

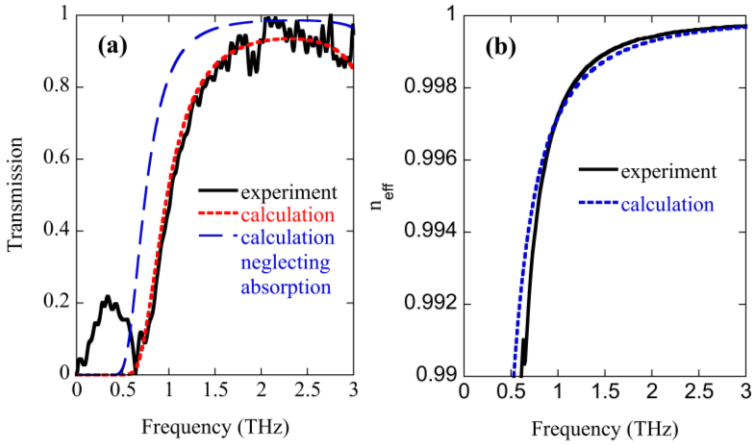

Fig. 3. (a) Measured amplitude transmission coefficient of a 13.5 cm long guide with 36 μm films separated by 2.0 mm (solid black curve). The dotted curve is the transmission calculated using Eq. (1). The dashed curve is a calculation neglecting dielectric absorption. (b) Measured and calculated (using Eq. (3)) effective refractive index.

The transmitted spectra predicted using Eq. (1) are compared with experiment in Fig. 2(b). The spectra are approximately calculated by multiplying the reference spectrum in Fig. 2(b) by $1-\exp(-\alpha_E L)$ where L is the guide length and are scaled vertically so as to overlap the experimental data. Even though the frequency dependence of the coupling efficiency is not taken onto account, there is good qualitative agreement with experimental results for the wavelength dependence except in regions of very high loss where the measurements are limited by the dynamic range of the TDTS apparatus. As a further check the calculated absolute transmission for a guide comprised of two 36 μm thick, 13.5 cm long films separated by 2 mm is compared with experiment in Fig. 3(a). The experimental data was obtained by dividing the response of two guides with lengths of 10 cm and 23.5 cm so as to remove the

need to consider the coupling efficiency when estimating the transmission coefficient. The first resonant loss band of this guide is at 3.3 THz, which lies just outside the experimental frequency range. Given the ±0.05 mm tolerance on the film separation and the fact that the experimental frequency range does not strictly satisfy the λ/h <<1 criterion for validity of Eq. (1), there is good quantitative agreement between experiment and calculation except below 0.7 THz where TM_0 core guidance fails and the largest contribution to the transmitted signal comes from the surface modes mentioned earlier and which are not described by Eq. (1).

The effective refractive index of the waveguide obtained from the measured spectral phase is shown in Fig. 3(b). Except close to transmission resonances, the field of the guided mode is small at the dielectric boundary and, neglecting absorption, n_{eff} can be well approximated by [24]

$$n_{eff} = k_o \left(1 - \left(\frac{m\lambda}{2h} \right)^2 \right)^{0.5} . \qquad (3)$$

Equation (3) is compared with the experimental data in Fig. 3(b) and shows good agreement.

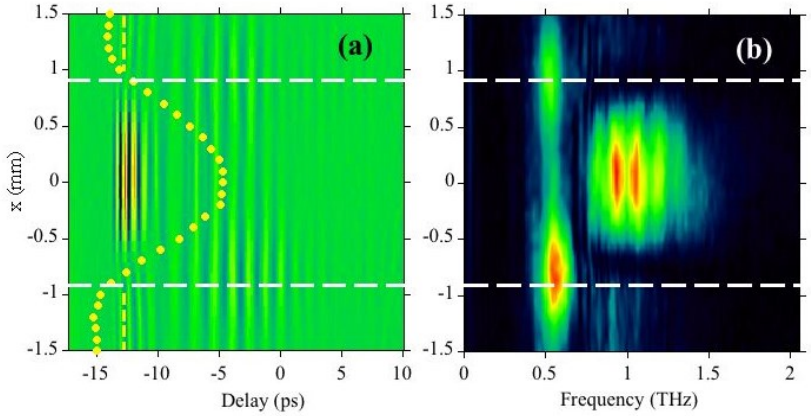

Fig. 4. (a) Time domain electric field map for translation along the *x*-axis for a parallel dielectric film guide with a film separation of 1.8 mm and film thickness of 36 μm. Red corresponds to positive signal and blue to negative. The symbols show the *x*-profile of the field at -12.8 ps and the vertical dashed lines indicate zero field. (b) Corresponding spectral amplitude map. The horizontal dashed lines show the film positions.

Anti-resonant guiding gradually becomes ineffective as the frequency is reduced below the first loss resonance due to an increase in film transmission with increasing transverse wavevector, as is evident in Figs. 2 and 3. This is exacerbated by dielectric absorption, as indicated in Fig. 3(a). To explore this failure of guiding in more detail, the spatial field distribution at the output end of a waveguide with a film separation of 1.8 mm and film thickness of 36 μm was mapped by scanning the detector with attached aperture across the output 'face' of the guide. The *x* component of the THz field is shown as space-time and space-frequency maps in Figs. 4(a) and 4(b) respectively. Above ~0.7 THz, the major fraction of the fundamental leaky TM_0 core mode is guided in the gap between the dielectric films by the ARROW mechanism. A small difference in time delay of ~0.5 ps between the electric fields in the core and outside the cladding at a delay of -12 ps confirms that the latter is leakage from the core.

The frequency domain map in Fig. 4(b) clearly displays spectrally and spatially distinct modes. The higher frequency mode is confined in the core, whilst narrower band, lower frequency modes are guided by the individual films. The vertical striations in Fig. 4(b) reflect a spectral amplitude variation of ~10% and are an artifact of the relatively short time window used to acquire the image. We also examined the time-domain signals along the *y*-axis (not

shown) and these displayed a frequency independent Gaussian amplitude profile extending over the width of the input beam. We conclude that at high frequencies a TM_0 mode is guided between the parallel dielectric films by the ARROW mechanism and that at lower frequencies guiding takes place predominantly in the thin films. We discuss this cross-over in more detail in section 4.

The radiation leakage rate from the core can be suppressed by interference between Fresnel reflections from additional air-spaced cladding surfaces, mirroring the effect of adding extra rings of tubes or an outer jacket in hollow core anti-resonant reflection fibres [14,25]. In the case that the cladding consists only of a thick jacket spaced from the core by a distance d, minimum loss occurs when the Bragg condition is satisfied and

$$d = \frac{(2q+1)\lambda}{4\sqrt{1-n_{eff}^2}} \tag{4}$$

where q=0,1,2 … and n_{eff} is the TM_0 mode index. Using Eq. (3) it is easily shown that for a planar guide Eq. (4) is satisfied if d is an odd multiple of $h/2$. In a cylindrical symmetry guide the condition is that d=0.65a where a is the core radius [26]. Adding additional, appropriately spaced thin wall films further reduces fundamental core mode loss but the benefit diminishes rapidly with increasing number of layers. The prediction of Eq. (4) was experimentally verified by adding 6 mm thick, HDPE cladding plates to a guide consisting of 36 μm thick films with a 2 mm spacing, as shown in Fig. 1. The spectrum of the core mode on the optical axis at the end of the guide was measured as a function of the film-plate separation d and the variation of the peak spectral amplitude at 1.1 THz is shown in Fig. 5. The beneficial effect of the extra cladding on reducing the loss when Eq. (4) is satisfied is clear.

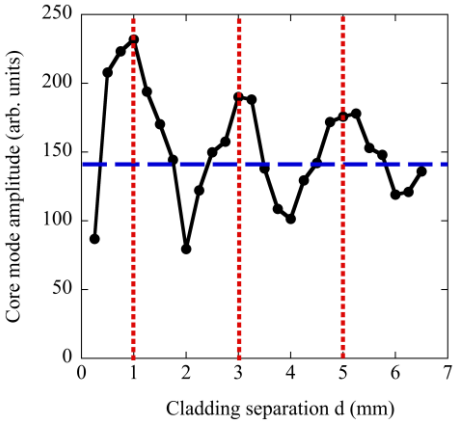

Fig. 5. Measured amplitude of TM_0 mode at x=0 and 1.1 THz as a function of the separation d between the thick cladding plates and the thin guiding films. The vertical dotted lines indicate the calculated loss minima values of d and the dashed horizontal line shows the amplitude when the outer cladding is removed.

3. Guiding in single films

Guiding by total internal reflection in thick single plastic films of HDPE has previously been investigated using TDTS by Mendis and Grischkowsky [27]. We used similar hyper-hemi-cylindrical lens coupling techniques to study the fundamental TM_0 mode in thin polyester films with thicknesses between 12 μm and 75 μm. This mode, like the leaky core mode of the parallel film guide, has no cut-off different from zero. Knife blades were placed very close to the input lens on both sides of the film and a 500 μm wide slit was attached to the cylindrical lens on the receiver side to discriminate against unguided radiation. Figure 6(a) shows transmitted spectra for films of different thickness but the same length of 13.5 cm. The thinner

films in Fig. 6(a) guide with larger transmission at higher frequency because a greater fraction of the field is in air. The spectra for the 36 μm and 50 μm thick films are very similar to the low frequency components in Figs. 2(b) and 3(a), confirming the presence of cladding modes in the parallel film guides.

Ignoring losses due to scattering at film imperfections, the TM_0 field attenuation coefficient in the $t<<\lambda$ limit has been shown to be [28]

$$\alpha_E = \frac{t^2 k_o^2 (n^2 - 1)\alpha_d}{4n^5}. \tag{5}$$

Cut-back measurements on 36 μm thick films were performed to compare the transmission loss with Eq. (5). The measured power attenuation was 2.0±0.2 dB/cm at 0.8 THz and 0.88±0.05 dB/cm at 0.5 THz. These values agree well with the calculated values of 2.2 dB/cm and 0.85 dB/cm for n=1.6 and a_d=18 cm^{-1}. The frequency dependence of the coupling of free space beams to very thin films makes it difficult to reliably compare the detailed shape of the transmission spectra in Fig. 6(a) with theory but the general trends are consistent with Eq. (5).

The dispersion relation for a TM mode can be derived from the transverse resonance condition [28]

$$k_o t\sqrt{n^2 - n_{eff}^2} - 2\phi = m\pi \tag{6}$$

where m is the mode index, 2ϕ is the phase shift for total internal reflection at the film's surfaces and

$$\phi = \tan^{-1}(n^2\sqrt{n_{eff}^2 - 1}\,/\sqrt{n^2 - n_{eff}^2}). \tag{7}$$

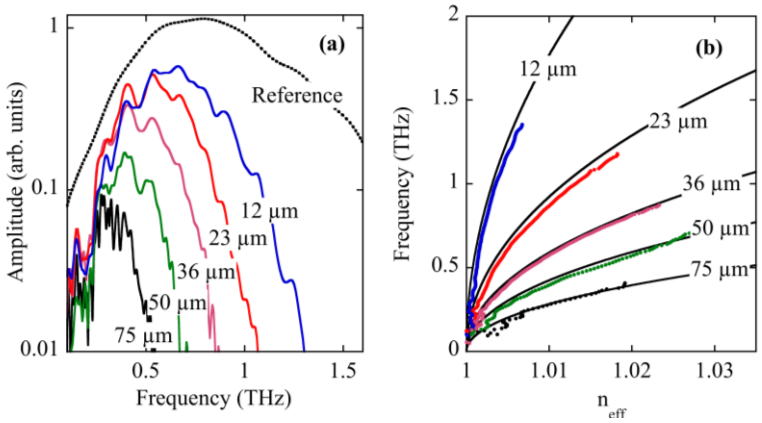

Fig. 6. (a) Spectra obtained after transmission along 13.5 cm polyester films of various thickness. A common vertical scale is used for all data. (b). The corresponding dispersion curves plotted as a function of effective index. Solid lines are calculations and points are measurements.

Figure 6(b) shows good agreement between n_{eff} calculated using Eqs. (6) and (7) and the experimental values obtained from analysis of the spectral phase for a range of film thicknesses. The field distribution along the x-axis was also measured for the 12 μm thick film, and is shown as a spectral amplitude map in Fig. 7. The majority of the field is clearly guided in the air surrounding the film, with a frequency dependent spatial extent showing closer binding of high frequencies to the dielectric. The latter is quantified by the white points in Fig. 7 which show the frequency variation of the 1/e amplitude fall-off distance.

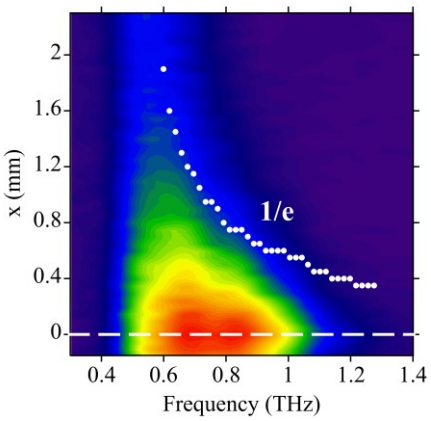

Fig. 7. Spectral amplitude map of radiation guided by a single 12 μm thick polyester film. The white dots indicate the 1/e amplitude fall-off distance. The dashed line shows the position of the film.

4. Effect of film separation on core and surface modes

Figure 8(a) shows a time domain map obtained by varying the separation of parallel, 36 μm thick films with the detector positioned on the optical axis, half way between the films. The core and surface modes are evident at small and large delay respectively. The high frequency core mode is differentiated at large separations by its faster oscillations (before a delay of ~5.0 ps) and becomes weaker as the films move closer together. On the other hand, the surface modes on the cladding films, which dominate the time domain signal after 5.0 ps, are not strongly affected by the film separation except when it is small enough for significant overlap of a wave guided on one film with the material of the other. This gives rise to the pronounced curvature in the amplitude map in Fig. 8(a) for film separation below 1.5 mm, presumably because greater material overlap leads to larger effective refractive index and thus a shift to larger time delay.

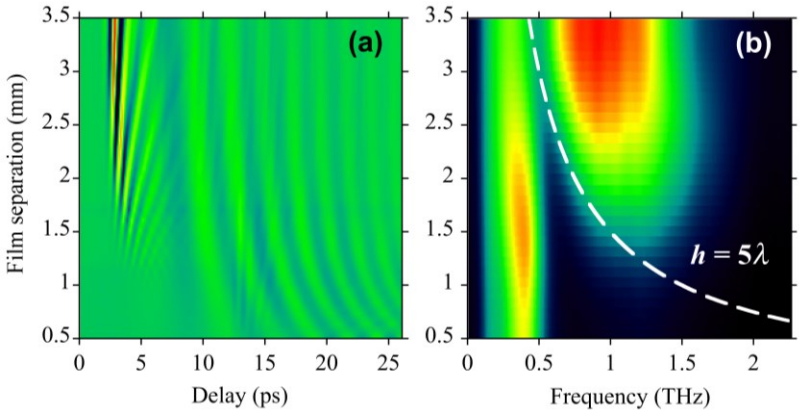

Fig 8. (a) Experimental amplitude-time map showing the effect of changing the film separation. The film thicknesses are 36 μm. (b) Frequency domain map corresponding to (a).

Figure 8(b) shows the frequency domain map corresponding to Fig. 8(a). A breakdown of core guidance and a transition to dominant film guidance when h decreases below roughly 5λ is evident. The calculated behavior of the core mode transmission is shown in Figs. 9(a) and 9(b). The curves in Fig. 9(b) are obtained by multiplying the transmission calculated using Eq. (1) in Fig. 9(a) by the reference spectrum in Fig. 2(b). Although the frequency dependence of

the coupling to the waveguide is not taken into account, the agreement between Figs. 8(b) and 9(b) is good.

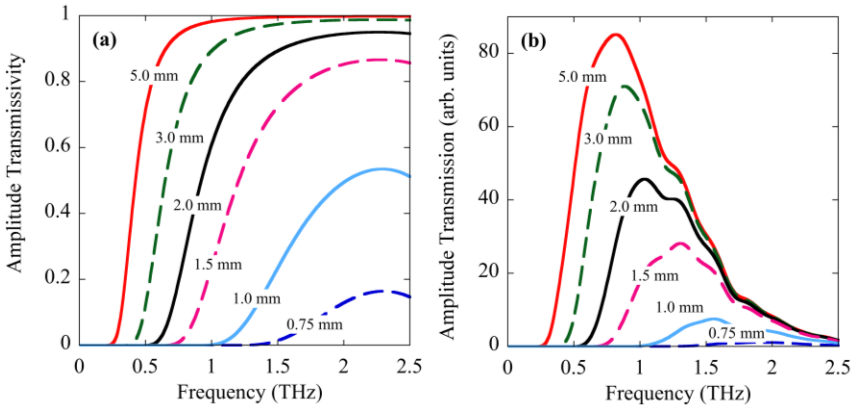

Fig. 9. (a) Amplitude transmissivity for a 13.5 cm long waveguide with 36 μm film thickness and the film separations shown. calculated using Eq. (1). (b) Transmitted spectra obtained by multiplying the system reference spectrum by the curves in (a).

5. Conclusions

We have studied THz waveguiding between parallel dielectric films, in particular the breakdown of anti-resonant reflection optical waveguiding (ARROW) and the transition to total internal reflection guiding in the individual films as the film separation is reduced and the effect on the transmission of adding variably spaced cladding layers. The frequency dependence of the core and surface mode attenuation and dispersion are well described by simple analytical models that, with slight modification, should work equally well for cylindrical geometry guides. The results demonstrate the power of the THz time domain imaging technique for studying waveguide modes.

Acknowledgment

We thank the UK Engineering and Physical Science Research Council for funding under grant EP/J007595/1.